Optimal management of coupled shared autonomous electric vehicles and power grids: potential of renewable energy integration

Xianyi Yang, Adam Abdin, Jakob Puchinger

Optimal management of coupled shared autonomous electric vehicles and power grids: potential of renewable energy integration

Yang Xianyi[a], Adam Abdin[b,*], Jakob Puchinger[c,b]

[a] *Beihang University, 37 Xueyuan Road, 100191, Beijing, China*
[b] *Université Paris-Saclay, CentraleSupélec, Laboratory of Industrial Engineering, 3 rue Joliot Curie, Gif-sur-Yvette, 92290, France*
[c] *EM Normandie Business School, Métis Lab, 30-32 rue Henri Barbusse, Clichy, 92110, France*

Abstract

Shared Autonomous Electric Vehicles (SAEVs) are pivotal for future transportation, offering both promise and challenges upon integration with the power grid. This symbiosis augments power system flexibility, stability and reliability through Vehicle-to-Grid (V2G) services, and optimize transportation efficiency. However, it amplifies the demand for robust charging infrastructure and electricity power during peak periods. This paper proposes a framework employing a sequential receding horizon optimization approach to manage SAEV mobility and charging dynamics. Focused on maximizing transportation service quality while ensuring power grid stability, the model accommodates dynamic trip requests and electricity generation, utilizing a rolling horizon algorithm. Notably, the study explores the potential of SAEVs in fortifying the integration of renewable energy resources (RES) into the power grid. Our research strives to equip policymakers and system planners with a robust tool for crafting efficient and sustainable future urban transportation and energy systems.

Keywords: Shared Transportation, Autonomous Electric Vehicles, Sequential optimization, Optimal Charging scheduling

*Corresponding author
Email address: adam.abdin@centralesupelec.fr (Adam Abdin)

1. Introduction

Increasing car ownership and usage is exacerbating traffic and parking congestion, as well as greenhouse gas emissions and air pollution (Zhou et al., 2020). Car-sharing services are expected to mitigate these problems (Ikezoe et al., 2020; Wang and Liao, 2021). More benefits can be offered if car-sharing is served by autonomous electric vehicles, such as the elimination of the time spent on parking and the improvement of the availability, accessibility, and affordability of sharing services (Iacobucci et al., 2018a; Vosooghi et al., 2019). Shared autonomous electric vehicles (SAEVs) are expected to become a cornerstone for future transportation, with significant impacts on urban mobility and energy consumption (Grazia Speranza, 2018). According to Fulton (2018), SAEVs could cut transportation energy use by 70%, CO2 emissions by 80%, and transportation costs by 40%, achieving savings approaching $5 trillion per year globally by 2050, compared to the current private vehicle ownership dominant transportation system. However, the proliferation of SAEVs could impose a significant charging burden on the grid, increasing localized power load fluctuations, as well as operational difficulties and higher operating costs for power system dispatch due to the uncertainty of when and where SAEVs are charged (Yao et al., 2022). The electrification of the transportation system leads to changes on the demand side of the grid system; meanwhile, the increasing renewable energy mandates are leading to the replacement of large-scale, slow-ramping, and dispatchable power plants with smaller non-dispatchable renewable energy resources (RES) such as solar and wind power plants on the generation side (Abdin and Zio, 2018). Concerns regarding environmental protection and sustainable development have resulted in there being a critical need for cleaner energy (Azzopardi, 2014). According to the "World Energy Outlook 2022", the share of global renewable energy resources in electricity supply was 29% by 2021, and it was expected to increase to at least 43% by 2035 and 65% by 2050 (IEA, 2022). However, the amount of electricity produced from these sources fluctuates greatly over time (Heide et al., 2010), and their forecast is often unpredictable (Mwasilu et al., 2014). This poses a significant challenge when it comes to integrating renewable energy resources into the power grid system (Anees, 2012). The

intermittency of renewable energy supply can easily disrupt the power grid's balance and lead to supply security risks. Efforts must, therefore, be undertaken to manage the power grid system in a reliable and cost-effective manner.

It is predicted that the widespread adoption of EVs could serve as one of the demand responses that can significantly facilitate the integration of intermittent renewable energy resources in the grid if they are managed well (Motta et al., 2023). EVs can absorb the surplus power through different charging schemes or can deliver power to the grid in low power availability scenarios, therefore leveling the power grid operations (Richardson, 2013). This is achieved via the proper development of vehicle-to-grid (V2G) schemes. However, regular or private EVs are individually owned, which makes them generally unavailable for demand response at all times. In contrast, SAEVs are managed by centralized control systems that can efficiently adjust to power demand and supply changes by integrating real-time data from the power grid and the vehicle fleet. This makes them easier to control and optimize for fast, large-scale demand response, potentially enabling easier and higher penetration of renewable energy resources by increasing grid flexibility (Fernandes et al., 2012).

There are many studies addressing the V2G-power system integration problem at various levels, including different kinds of regulatory, technical, or pricing practices (Wolinetz et al., 2018). However, these studies extensively focus on privately owned vehicles with predictable charging locations and patterns. However, when it comes to SAEVs, both travel and charging activities are uncertain and dynamic, necessitating careful consideration in fleet operations since an unplanned charging strategy could also affect the service availability of SAEVs, resulting in higher passenger waiting times and less vehicle utilization (Zhang and Chen, 2020; Vosooghi et al., 2019). Hence, some recent research works developed transportation models of SAEV that consider factors in the power grid to investigate the benefits of co-managing both systems simultaneously. This includes managing aspects such as the electricity price, layout of charging infrastructure, and the power grid service (Iacobucci et al., 2018b). However, the potential of SAEVs to improve power grid stability and fa-

cilitate larger integration of intermittent renewable energy has been largely overlooked. In addition, existing studies addressing V2G integration in transportation models do not take into account the detailed configurations and constraints in the power grid, such as capacity constraints, transmission line topologies, and related parameters. Properly modeling these aspects is crucial to achieving accurate results in the co-management of the electrified transportation system and the power grid. By considering these elements, SAEV can be optimized to operate without compromising the stability and reliability of the grid.

To investigate new control and optimization algorithms to better manage the integration of SAEVs and renewable energy resources into the power grid, in this paper, we extend the SAEV model proposed in Zhang et al. (2016) by coupling it with a DC Optimal Power Flow (DC-OPF) model representing detailed power grid operations. Furthermore, we incorporate the intermittency of renewable generation within the optimization framework by adding variables that record the charging demand of vehicles and the gap between energy demand and supply, as well as several power grid variables and constraints, including demand and generation balance, generation limits, ramp rate limits, voltage angle limits, and power flow limits. The SAEV-power system (SAEV-PS) coupled model is formulated as a mixed integer linear program (MILP) that efficiently meets the traveler's needs while ensuring power grid stability. Additionally, we consider dynamic trip requests and electricity generation that vary over time and propose a rolling horizon optimization algorithm to solve this optimization problem. For this, the problem is decomposed into several subproblems that are sequential in time.

The rest of the paper is organized as follows. A literature review and the paper contributions are presented in Section 2. The model developed is described in detail in Section 3. The solution algorithm is explained in Section 4. In Section 5, we build a case study using Beijing's traffic, grid, and climate data. Furthermore, we apply the model and algorithm to the case study and conduct calculations for the model validation, the demonstration of the potential of SAEVs in improving the integration of renewable energy resources into the grid, the comparison between the SAEV transportation model and the SAEV-PS coupled model,

and a sensitivity analysis on key model parameters such as discharging rate, consumption rate and battery capacity. The results are discussed in Section 6, illustrating the usefulness, necessity and efficiency of our proposed modeling and optimization framework in finding optimal solutions for the coupled SAEV-power grid management problem. Finally, Section 7 presents our conclusions and future work.

2. Literature review and paper contributions

This section reviews the relevant literature on managing EVs and SAEVs fleet operations. We show that existing literature focuses on optimizing the mobility performance of SAEVs but neglects the impact of managing charging behavior on the power grid performance. Reversely, we show that most of the literature that considers the co-management optimization of EV charging and its impact on the power grid does not take into account the detailed modeling of transportation demand patterns. Some literature provides an integrated approach to modeling and optimizing the SAEV-power grid integration but does not provide a modeling framework to evaluate the impact of SAEVs on the integration of intermittent renewable energy sources. This section comprehensively reviews existing studies covering these topics and summarizes the research gaps and our original contributions.

2.1. Optimizing mobility performance of SAEV

A large body of literature on the operation of SAEVs has focused on optimizing the SAEV mobility performance. Generally, in this case, the impact of the charging behavior on electric power systems is overlooked. Some research works used agent-based models to simulate the transport operation of SAEVs (Bischoff and Maciejewski, 2016; Liu et al., 2018; Zhang et al., 2015). Other works developed mathematical programming models to represent the operation of SAEVs and optimize the transportation behaviors of vehicles (Ma et al., 2017; Li et al., 2016; Kang and Levin, 2021). Their results indicate the significant potential benefits of SAEVs in improving mobility and sustainability in the current transportation system, but the charging behavior's impact on electric power systems is ignored.

2.2. Vehicle-grid integration problems

Although SAEVs have been demonstrated to be efficient in terms of transportation performance, their high adoption rate in the transportation system can result in a "peak on peak" effect on the power grid (Huang et al., 2013). This phenomenon, along with the intermittency of renewable energy production, could lead to severe power system instabilities (Abdin and Zio, 2019; Abdin et al., 2022), as observed in southern Norway in 2017 (Noel et al., 2017). Several research works have focused on studying the impact of EVs on the grid and provided charging management strategies, which gives valuable insights into vehicle-grid integration problems. However, most studies focus on the case of managing privately-owned vehicles, which have predictable travel patterns due to personal mobility needs and preferences (Yi and Bauer, 2016; Khodayar et al., 2013; Xu and Pan, 2012; Ding et al., 2022; Han et al., 2010; Sun et al., 2019). As a result, in these research works, vehicles' charging demands are often treated as exogenous stochastic inputs following a priori-defined probability distributions.

2.3. Vehicle-grid integration problems of SAEV

In contrast, SAEVs are operated by mobility service providers and are shared among multiple users, which means they require not only charging management but also mobility management, referred to as Autonomous Mobility-on-Demand (AMoD) problem. This problem includes vehicle assignment and relocation management, involving matching the right vehicle to the proper customer demand and defining the optimal vehicle trajectory from one location to another to balance supply and demand (Özkan, 2020; Bélanger et al., 2019). Therefore, regarding vehicle-grid integration in the context of SAEV, some research developed transport models of SAEV that consider power grid variables to investigate the co-management of both systems. This includes considering electricity prices, which reflect demand pressures on the grid in the time dimension, and the layout and location of charging infrastructure to optimize stress on the grid in the spatial dimension. Additionally, some studies explore the potential for SAEVs to provide grid services, such as operating reserves and grid storage, with energy demand determined by mobility behaviors.

For instance, Iacobucci et al. (2018a) optimizes the operation of SAEV in a node-based map considering electricity price and grid reserve capacity requirements. The vehicles in the model are assigned to trip requests by a Hungarian algorithm. A heuristic-based demand-response strategy based on electricity price signals from the grid is used for charging. The study found that incorporating electricity prices into the charging strategy of SAEVs can lower the cost of their transport, and SAEVs can potentially serve as operating reserves for the grid. Chen et al. (2016) optimizes the operation of SAEV in a graph-based area under various scenarios of vehicle range and charging infrastructure layout based on an agent-based model. The greedy search algorithm is applied to dispatch SAEV to trip requests and charging stations, and the most efficient relocation strategy combination proposed by Fagnant and Kockelman (2014) is used to optimize vehicle relocation. The results demonstrate that the layout of the charging infrastructure and the range of the vehicles significantly influence the vehicle fleet size. The study in Vosooghi et al. (2020) presents a framework for simulating SAEVs and their charging infrastructure in a cell-based map using an agent-based model that assumes dynamic demand and network congestion. A dispatching algorithm developed by Bischoff and Maciejewski (2016) allocates vehicles to trips. The simulation examines various factors, such as locations of charging stations, type and number of charging outlets, SAEV battery capacity, and battery swapping technology. The results show that the performance of SAEVs is highly dependent on the charging infrastructure. The study presented in Bauer et al. (2018) developed an agent-based model to simulate SAEVs in a node-based district. The model assigns trips to the nearest available vehicle and relocates idle vehicles within a 10-minute radius of trip requests. An iterative process was used to optimize the positioning of charging stations, starting with chargers located on all nodes and eliminating the least used chargers in each iteration. Through sensitivity analysis, the study determined the optimal battery size and number of charging stations required to minimize the costs associated with the operation of SAEVs.Loeb et al. (2018) presents an optimization model that evaluates the performance of the SAEV system in a node-based region. The simulation considers various factors such as battery range, charging time, fleet size, and charging

station placement to identify optimal strategies for maximizing system performance. Furthermore, a dynamic traffic assignment algorithm presented by W Axhausen et al. (2016) was employed to optimize customers' trip patterns. The study reveals that charging stations become scarce as vehicle range increases. Zhang et al. (2016) proposes a mathematical programming model to optimize the mobility service of SAEVs in a node-based traffic network. The problem is formulated as a mixed-integer linear program (MILP) and solved using a model predictive control (MPC) approach. The objectives of the problem are to maximize the service to all waiting customers and relocate SAEVs in an efficient manner. The model also considers charging constraints, with the placement of charging stations pre-set and different charging speeds compared. The study compares the proposed MPC algorithm with other vehicle dispatch algorithms and demonstrates its advantages of computational time and solution quality. Iacobucci et al. (2019) builds upon the work proposed in Zhang et al. (2016) by considering the charging and discharging of SAEVs and electricity prices. The results indicate that SAEVs have the potential to offer adequate energy storage to the grid and avoid grid congestion through dynamic pricing. A summary of the models and the elements considered in the relevant literature is provided in Table.1.

Table 1: Summary of the relevant literature on vehicle-grid integration problems of SAEV.

	Formulation	Road net	Power grid	Electricity price	Charging infrastructure	Power grid service
Iacobucci et al. (2018a)	Nearest neighbor assignment	Yes, based on nodes	No	Yes	The position of charging station	operating reserve
Chen et al. (2016)	Agent-based	Yes, based on graph	No	No	The position of charging station and the type of chargers	No
Vosooghi et al. (2020)	Agent-based	Yes, based on cells	No	No	The position of charging station, the type of chargers and the number of outlets	No
Bauer et al. (2018)	Agent-based	Yes, based on nodes and with traffic condition	No	No	The position of charging station, the type and the number of chargers	No
Loeb et al. (2018)	Agent-based	Yes	No	No	The position of charging station and the type of chargers	No
Zhang et al. (2016)	MILP	Yes, based on nodes	No	No	Charging rate	No
Iacobucci et al. (2019)	MILP	Yes, based on nodes	No	Yes	No	Energy storage

2.4. Contributions

In conclusion, several studies have investigated the mobility performance of SAEVs and demonstrated the proposed models' efficiency in optimizing transportation-related decisions. However, those studies have typically overlooked the impact of SAEV charging on the power grid, and explicit modeling of the power system is not considered. Given that a high share of EVs may pose significant challenges to the power grid, much research has been conducted on the vehicle-grid integration problem, but most have focused on private vehicles and the charging scheduling problem. These studies typically ignore the transportation modeling of the vehicle and treat the vehicle's charging demands as exogenous stochastic inputs, which is unacceptable when it comes to SAEVs because mobility performance needs to be guaranteed when their charging strategy is managed. Hence, some works studied the operational management of SAEVs by considering the electric price, charging infrastructure, and grid services based on the transportation model of SAEV. However, to the best of our knowledge, no existing study has considered a modeling and optimization approach that considers the co-management of SAEVs with the power system, particularly to study the potential of this co-management on the integration of intermittent renewable energy sources. Therefore, this study attempts to address these knowledge gaps and has the following contributions:

- First, we propose a novel modeling and optimization framework to manage the coupled SAEV mobility service and its interaction with the electric power grid. Our novel modeling approach focuses on analyzing the potential of SAEVs to improve the integration of renewable energy in the power grid. The model provides novel extensions of state-of-the-art SAEV transportation models, including flexible charging state variables and adapted objective functions. Additionally, it is coupled with a DC optimal power flow model (DC-OPF model) by adding several power grid variables and constraints, including demand and generation balance, generation limit, ramp rate limit, voltage angle limit, and power flow limit. These considerations improve the model and fill the gap in the field.

- Second, we propose a rolling horizon solution algorithm capable of solving the resulting

mathematical programming model under realistic sequential and dynamic trip requests and renewable energy availability scenarios. While the algorithm shares similarities with the traditional rolling horizon algorithm, it had not previously been applied to the specific problem that integrates transportation system and power grid within a dynamic setting. The proposed rolling horizon algorithm is shown to be capable of achieving optimal solutions with high computational efficiency.

- Third, using the proposed framework, a real-world case study based on the Taxi GPS data, power grid configuration, and climate data of Beijing in China is employed to demonstrate the usefulness, necessity and efficiency of our proposed modeling and optimization framework, as well as the potential of SAEV to help integrate renewable energy resources into the grid. The results give valuable insights into the topic of optimal management of electrified mobility systems and electric power grids.

3. Model

This section presents the model developed in our work. We provide novel extensions to the SAEV AMoD model presented in Zhang et al. (2016) to integrate the DC-OPF model and the AMoD problem within a single optimization. Table 2 summarizes the variables, parameters, and sets used in the model. The variables are divided into two categories: state variables and decision variables. The state variables reflect the state of the system over time, and the decision variables represent the control actions to be optimized. Figure 1 illustrates the decision-making process of a single vehicle, showcasing the evolution of all state variables pertaining to the vehicle. This includes decisions regarding movement or parking, charging and discharging, as well as the changes in energy levels over time.

3.1. Shared autonomous electric vehicle (SAEV) operational model

The SAEV operational model is proposed to minimize the number of waiting passengers, with penalty terms to ensure vehicles do not rebalance for no reason. This is shown in Eq.(1), where t represents the time steps within the set T, N represents the set of nodes, and V

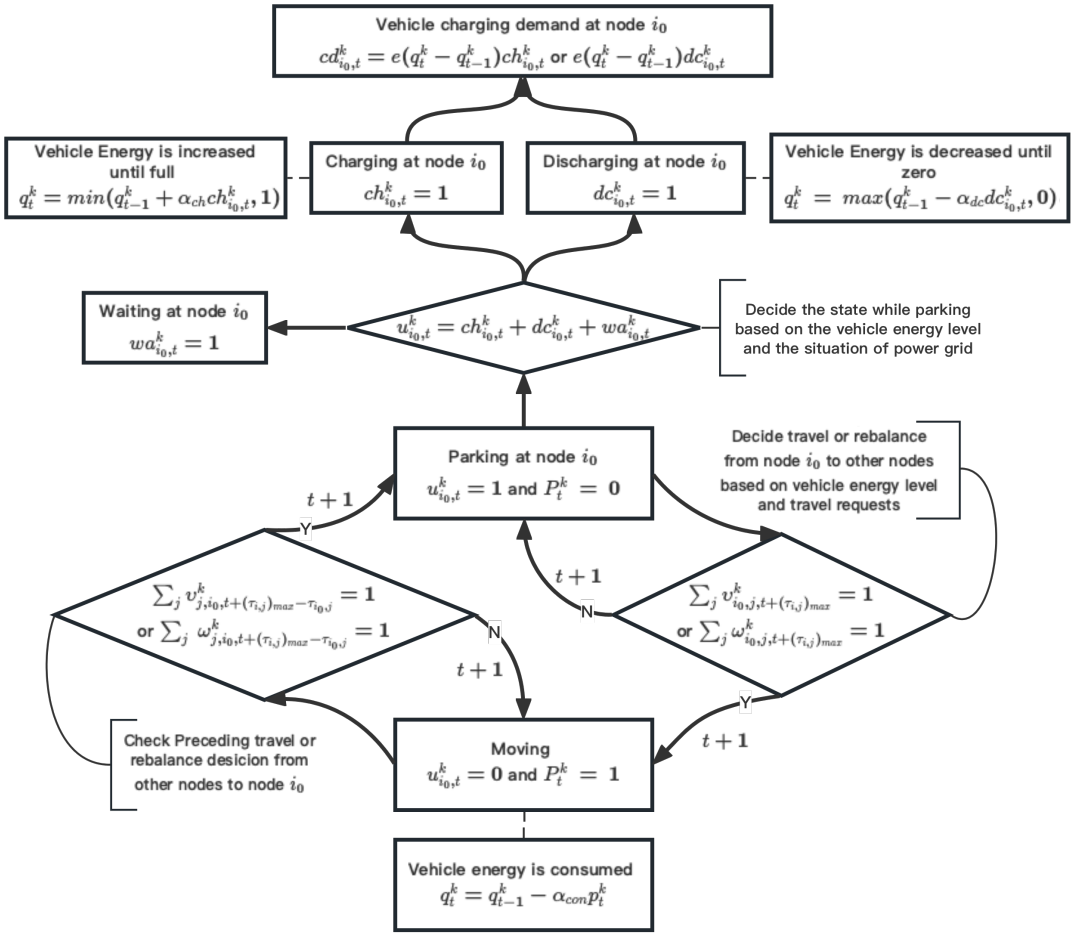

Figure 1: The decision-making process of the vehicle k

Table 2: Variables and parameters

Sets	Data type	Definition
T		Set of time t
N		Set of nodes i
V		Set of vehicles k
Parameters		
$c_{i,j,t}$	Integer	Number of new customers starting at node i with destination j at time t
$cd_{i,t}$	Real Number	The charging demand at node i at time t
$d_{i,j,t}$	Integer	Number of waiting customers starting at node i with destination j at time t
$\alpha_{ch}, \alpha_{dc}, \alpha_{con}$	$\in [0,1]$	Electricity charging, discharging and consumption rate
$\tau_{i,j}$	Integer	Distance between node i and j measured by time step
ρ_d	Positive Real	The weight of objective term
$\varphi_\omega, \varphi_{sg}$	Positive Real	The penalty weight of penalty terms
g_i^{max}	Positive Real	limitation of electricity generation at node i
$\bar{\theta}$	Positive Real	limitation of difference in voltage angle
$\chi_{i,j}$	Positive Real	Inductance of arc between node i and j
$f_{i,j}$	Positive Real	limitation of power flow
RD_i, RU_i	Positive Real	limitation of generation ramp rate
e	Positive Real	Battery Capacity
State Variables		
$u_{i,t}^k$	Binary	Parking status of vehicle k at time t
q_t^k	$\in [0,1]$	Charging level of vehicle k at time t
p_t^k	Binary	Moving status of vehicle k at time t
$f_{i,j,t}$	Real Number	The power flow in grid arc between node i and j at time t
$cd_{i,t}^k$	Real Number	The charging demand of vehicle k at node i at time t
$cd_{i,t}^{SAEV}, cd_{i,t}^{Ret}$	Real Number	The charging demand of SAEV and residents
Decision Variables		
$wa_{i,t}^k$	Binary	Waiting status of vehicle k at time t
$v_{i,j,t}^k$	Binary	Travelling decision of vehicle k from node i to node j at time t to pick-up passengers
$\omega_{i,j,t}^k$	Binary	Travelling decision of vehicle k from node i to node j at time t to rebalance
$ch_{i,t}^k$	Binary	Charging decision of vehicle k at time t
$dc_{i,t}^k$	Binary	Discharging decision of vehicle k at time t
$g_{i,t}$	Real Number	The electricity generation at node i at time t
$g_{i,t}^{con}, g_{i,t}^{rew}$	Real Number	The generation of conventional energy and RES
θ_i	Real Number	Voltage angle at ndoe i
$sg_{i,t}$	Real Number	Electricity spillage at node i at time t

represents the set of vehicles. ρ_d is the weight of objective term. ϕ_ω is the penalty weight.

$$\min_{\substack{i,j\in N \\ t=0,1\cdots T \\ k\in V}} \rho_d \sum_{t,i,j} d_{i,j,t} + \varphi_\omega \sum_{i,j,k,t} \tau_{i,j} \omega_{i,j,t}^k \tag{1}$$

$d_{i,j,t}$ denotes the number of waiting passengers at time t who want to travel from node i to node j. The state evolution of this variable is expressed by Eq.(2). The number of waiting passengers at the next time step $t+1$ equal to the number of currently waiting passengers, plus the number of newly arrived passengers $c_{i,j,t}$, minus the sum of picked-up passengers $\sum_{k\in V} v_{i,j,t}^k$. $v_{i,j,t}^k$ is a binary decision variable which is equal to 1 when vehicle k

picks up a passenger from node i to node j at time t, otherwise it is 0.

$$d_{i,j,t+1} = d_{i,j,t} + c_{i,j,t} - \sum_{k \in V} \upsilon^k_{i,j,t} \tag{2}$$

Similarly, the binary variable $\omega^k_{i,j,t}$ denotes the rebalancing decision of vehicle k. Rebalancing is a process by which idle vehicles adjust their positions to improve their services' efficiency. In contrast to privately owned electric vehicles, this is the most distinctive feature of autonomous vehicles.

The vehicle's moving status can be tracked by the binary variable p^k_t. It equals 1 when vehicle k moves from $t-1$ to t. The evolution expression is formulated by Eq.(3), where $\tau_{i,j}$ represents the distance (in terms of time steps) between nodes i and j. If there are decisions to pick up a passenger or rebalance itself for vehicle k at time t, the addition of the term, $\sum_{i,j \in N}(\upsilon^k_{i,j,t} + \omega^k_{i,j,t})$, represents the transition of p^k_t from 0 to 1. If the vehicle k is moving from node i with a mission assigned $\tau_{i,j}$ ago, it would stop at node j next time step. Hence, the subtraction of the term, $\sum_{i,j \in N}(\upsilon^k_{i,j,t-\tau_{i,j}} + \omega^k_{i,j,t-\tau_{i,j}})$, account for the change from 1 to 0.

$$p^k_{t+1} = p^k_t + \sum_{i,j \in N} (\upsilon^k_{i,j,t} + \omega^k_{i,j,t}) - \sum_{i,j \in N} (\upsilon^k_{i,j,t-\tau_{i,j}} + \omega^k_{i,j,t-\tau_{i,j}}) \tag{3}$$

Eq.(4) adds $(\tau_{i,j})_{max}$ to the time subscript of decision variables to solve the problem when $t - \tau_{i,j}$ is negative. Here, $(\tau_{i,j})_{max}$ signifies the maximum distance between all pairs of nodes. Although this adjustment may result in a discrepancy between the subscripts of decision variables and other variables (for instance, at the initial time step where t equals 0, the subscript of $\upsilon^k_{i,j,t+(\tau_{i,j})_{max}}$ is $(\tau_{i,j})_{max}$ while that of other variables is 0), it does not disrupt the synchrony of time, thereby maintaining the logical integrity of Eq.(3). Decision variables preceding the initial time are simply set to 0 during testing to ensure they do not impact calculations within the target time horizon.

$$\begin{aligned} p^k_{t+1} = p^k_t &+ \sum_{i,j \in N} (\upsilon^k_{i,j,t+(\tau_{i,j})_{max}} + \omega^k_{i,j,t+(\tau_{i,j})_{max}}) \\ &- \sum_{i,j \in N} (\upsilon^k_{i,j,t+(\tau_{i,j})_{max}-\tau_{i,j}} + \omega^k_{i,j,t+(\tau_{i,j})_{max}-\tau_{i,j}}) \end{aligned} \tag{4}$$

The variable p records the movement status of the vehicle, but not its specific location while in motion, which is irrelevant for our purposes. However, we do require knowledge of the stopping location in order to calculate the charging demand in that area. Therefore, we introduce the binary variable $u_{i,t}^k$ to capture this information. When vehicle k is waiting at the node i from $t-1$ to t, it is set to 1. The evolution expression is formulated in Eq. (5). It should be noted that $u_{i,t}^k$ and p_t^k cannot be equal to one simultaneously, as described in Eq. (10). If vehicle k decides to travel a passenger or rebalance at time t, then $u_{i,t+1}^k$ will become 0.

$$\begin{aligned} u_{i,t+1}^k = u_{i,t}^k &- \sum_{j \in N} (\upsilon_{i,j,t+(\tau_{i,j})_{max}}^k + \omega_{i,j,t+(\tau_{i,j})_{max}}^k) \\ &+ \sum_{j \in N} (\upsilon_{j,i,t+(\tau_{i,j})_{max}-\tau_{j,i}}^k + \omega_{j,i,t+(\tau_{i,j})_{max}-\tau_{j,i}}^k) \end{aligned} \tag{5}$$

To make the charging process more flexible, vehicles are assigned three state variables, $\mathrm{ch}_{i,t}^k$, $\mathrm{dc}_{i,t}^k$ and $\mathrm{wa}_{i,t}^k$, simulating three different behaviors when waiting at a node. All three variables are binary. The variable $\mathrm{ch}_{i,t}^k = 1$ indicates that vehicle k charges while waiting at node i. $\mathrm{dc}_{i,t}^k$ and $\mathrm{wa}_{i,t}^k$ denotes discharging and waiting without charging nor discharging, respectively. A new constraint is added since the vehicle can only be in one state while waiting at a charging node. This is formulated in Eq.(6).

$$u_{i,t}^k = ch_{i,t}^k + dc_{i,t}^k + wa_{i,t}^k \tag{6}$$

The electricity level of vehicle k is recorded with variable q_t^k, which varies between 0 and 1, indicating an empty and a full battery, respectively. The evolution is expressed by Eq.(7). α_{ch}, α_{dc} and α_{con} are, respectively, the charging rate, discharging rate, and consumption rate. They are defined as the percentage of energy evolution within a single time step relative to the battery capacity. The first part of Eq.(7) ensures that the charging level is limited to the upper and lower bounds. The term $\alpha_{con} p_{t+1}^k$ represents the electricity loss incurred while the vehicle is in motion. Constraints (8) and (9) guarantee that the vehicle cannot charge when the battery is fully charged and that it cannot discharge when the battery is

empty.

$$q_{t+1}^k = min\{max\{q_t^k + \alpha_{ch} \sum_{i \in N} ch_{i,t+1}^k - \alpha_{dc} \sum_{i \in N} dc_{i,t+1}^k, 0\}, 1\} - \alpha_{con} p_{t+1}^k \tag{7}$$

$$\sum_{i \in N} ch_{i,t+1}^k \leq M(1 - q_t^k) \tag{8}$$

$$\sum_{i \in N} dc_{i,t+1}^k \leq M q_t^k \tag{9}$$

Eqs.(10) to (14) are logical constraints in the model. Eq.(10) constraints each vehicle to be either moving or waiting. Eq.(11) specifies that a vehicle is either moving a passenger or rebalances. Eq.(12) limits the number of passengers to be transported to the maximum number of passengers waiting at a node. Eqs. (13) and (14) ensure that the charging level of a vehicle is sufficient to cover its travel to the required destination.

$$\sum_{i \in N} u_{i,t}^k + p_t^k = 1 \tag{10}$$

$$\sum_{i \in N} \left(u_{i,t+1}^k + \sum_{j \in N} \left(\upsilon_{i,j,t+(\tau_{i,j})_{\max}}^k + \omega_{i,j,t+(\tau_{i,j})_{\max}}^k \right) \right) = 1 \tag{11}$$

$$\sum_{k \in V} \upsilon_{i,j,t+(\tau_{i,j})_{\max}}^k \leq d_{i,j,t} + c_{i,j,t} \tag{12}$$

$$q_t^k \geq \upsilon_{i,j,t+(\tau_{i,j})_{\max}}^k \alpha_{con} \tau_{i,j} \tag{13}$$

$$q_t^k \geq \omega_{i,j,t+(\tau_{i,j})_{\max}}^k \alpha_{con} \tau_{i,j} \tag{14}$$

3.2. DC Optimal Power Flow Model (DC-OPF model)

In this part, a DC-OPF model is introduced. The concept of optimal power flow is proposed for preventing transmission line overloads in the power grid (Carpentier, 1979). In its classical version, this is a nonlinear, nonconvex optimization problem that is difficult to solve. Due to the computational difficulty of the OPF problem, some approximation methods exist in the literature. One of the most frequently used approximation methods is the DC-OPF model (Aigner et al., 2022), where the constraints are as follows: Eq.(15)

limits the electricity generation of each node. Eq.(16) balances the charging demand $cd_{i,t}$ and the electricity generation $g_{i,t}$. Eq.(17) constrains the ramp rate of generation between consecutive time steps. Eq.(18) sets the power flow magnitude and direction between nodes based on the difference in voltage angles and the susceptance of the transmission line. The maximum flow in each transmission line is limited by Eq.(19) in both power flow directions. Similarly, the voltage angle is constrained within the physical limits set in Eq.(20). Finally, the voltage angle for the selected reference node is set to zero, as indicated by Eq.(21). Eq.(22) balances the charging demand $cd_{i,t}$, power flow $f_{i,t}$ and the electricity generation $g_{i,t}$ at each node i.

$$g_i^{\min} \leq g_{i,t} \leq g_i^{\max} \tag{15}$$

$$\sum_{i \in N} (cd_{i,t} - g_{i,t}) = 0 \tag{16}$$

$$RD_i \leq g_{i,t+1} - g_{i,t} \leq RU_i \tag{17}$$

$$-2\bar{\theta} \leq \theta_{i,t} - \theta_{j,t} - \chi_{i,j} f_{i,j,t} \leq 2\bar{\theta} \tag{18}$$

$$-\bar{f}_{i,j} \leq f_{i,j,t} \leq \bar{f}_{i,j} \tag{19}$$

$$-\bar{\theta} \leq \theta_{i,t} \leq \bar{\theta} \tag{20}$$

$$\theta_{i^{ref}} = 0 \tag{21}$$

$$g_{i,t} + f_{i_{\text{in}},t} - f_{i_{out},t} - cd_{i,t} = 0 \tag{22}$$

3.3. Vehicle-grid Integration (VGI) model

To connect the SAEV model with the DC-OPF model, charging demand variables are added to the model and the expression is presented in Eq.(23). We assume that $cd_{i,t}^{SAEV}$ increases when any vehicle is charged at node i from t to $t+1$ and decreases when it is discharged. Node i is equivalent to a generator if $cd_{i,t}$ is a negative value, which provides electricity for other load nodes.

$$cd_{i,t}^{SAEV} = e \left(\sum_{k \in V} \left(q_{t+1}^k - q_t^k \right) ch_{i,t+1}^k + \sum_{k \in V} \left(q_{t+1}^k - q_t^k \right) dc_{i,t+1}^k \right) \tag{23}$$

Considering the intermittency of renewable energy electricity generation, variables recording the excessive electricity generation or electricity spillage, $sg_{i,t}$, are added in our VGI model. If $sg_{i,t}$ is negative, it means the power grid cannot meet the consumption, and an electricity shortage occurs. The electricity generation variables $g_{i,t}$ are separated into two parts: one is from renewable energy, $g_{i,t}^{rew}$, and the other, $g_{i,t}^{con}$ is from conventional generators such as coal and natural gas. The penetration rate of renewable energy in the power grid is determined by the proportion of $g_{i,t}^{rew}$ in $g_{i,t}$. Except for the charging demand of SAEV, residential charging demand, $cd_{i,t}^{ret}$ is considered as well. With these new variables, Eq.(16) and (22) are changed to (24) and (25). Eq.(26) constrains the charging behavior of SAEVs that they cannot charge when the power grid lacks energy. One more penalty term is added to the objective function, shown in Eq.(27). With this term, SAEVs are incentivized to stabilize the power grid's imbalance between power generation and consumption.

$$\sum_{i \in N} \left(cd_{i,t}^{SAEV} + cd_{i,t}^{ret} - g_{i,t}^{con} - g_{i,t}^{rew} - sg_{i,t} \right) = 0 \tag{24}$$

$$g_{i,t}^{rew} + g_{i,t}^{con} + f_{i_{in},t} - f_{i_{out},t} - cd_{i,t}^{ret} - cd_{i,t}^{SAEV} - sg_{i,t} = 0 \tag{25}$$

$$ch_{i,t+1}^{k} sg_{i,t} \geq 0 \tag{26}$$

$$\min_{\substack{i,j \in N \\ t=0,1 \cdots T \\ k \in V}} \rho_d \sum_{i,j,t} d_{i,j,t} + \varphi_\omega \sum_{i,j,k,t} \tau_{i,j} \omega_{i,j,t+(\tau_{i,j})_{max}}^{k} + \varphi_{sg} \sum_{i,t} \mid sg_{i,t} \mid \tag{27}$$

3.4. Linearization

There are two types of nonlinear constraints in the model. To facilitate the calculation, these nonlinear constraints are converted to linear constraints by a disjunctive constraints method.

The state evolution of vehicles' electricity level as Eq.(7) Is converted into Eqs.(28)–(40).

$$z_{1t}^{k} \geq \alpha_{ch} \sum_{i \in N} ch_{i,t+1}^{k} - \alpha_{dc} \sum_{i \in N} dc_{i,t+1}^{k} \tag{28}$$

$$z_{1t}^{k} \geq 0 \tag{29}$$

$$z_{1_t}^k \leq \alpha_{ch} \sum_{i \in N} ch_{i,t+1}^k - \alpha_{dc} \sum_{i \in N} dc_{i,t+1}^k + M \left(1 - u_{1_t}^k\right) \tag{30}$$

$$z_{1_t}^k \leq M u_{1_t}^k \tag{31}$$

$$z_{2_t}^k \leq 1 \tag{32}$$

$$z_{2_t}^k \leq q_t^k + z_{1_t}^k \tag{33}$$

$$q_t^k + z_{1_t}^k \leq z_{2_t}^k + M \left(1 - u_{2_t}^k\right) \tag{34}$$

$$1 \leq z_{2_t}^k + M \left(1 - u_{3_t}^k\right) \tag{35}$$

$$u_{2_t}^k + u_{3_t}^k \geq 1 \tag{36}$$

$$u_{1_t}^k \in \{0, 1\} \tag{37}$$

$$u_{2_t}^k \in \{0, 1\} \tag{38}$$

$$u_{3_t}^k \in \{0, 1\} \tag{39}$$

$$q_{t+1}^k = z_{2_t}^k - \alpha_{con} p_{t+1}^k \tag{40}$$

The expression of charging demand as Eq.(23) Is converted into Eqs.(41) to (46).

$$cd_{i,t} = \sum_{k \in V} cd_{i,t}^k e \tag{41}$$

$$cd_{i,t}^k \leq M \left(ch_{i,t+1}^k + dc_{i,t+1}^k\right) \tag{42}$$

$$cd_{i,t}^k \geq -M \left(ch_{i,t+1}^k + dc_{i,t+1}^k\right) \tag{43}$$

$$cd_{i,t}^k \leq q_{t+1}^k - q_t^k + M \left(1 - ch_{i,t+1}^k + dc_{i,t+1}^k\right) \tag{44}$$

$$cd_{i,t}^k \geq q_{t+1}^k - q_t^k - M \left(1 - ch_{i,t+1}^k + dc_{i,t+1}^k\right) \tag{45}$$

$$0 \leq cd_{i,t}^k \leq 1 \tag{46}$$

4. Solution Method

The idea of the rolling horizon algorithm is to solve the problem over a chosen planning horizon and use current prediction but to fix and effectively apply only a part of the optimized decisions. Then, for the next step, the system state and the predictions are updated, as in real-life situations, and the problem is solved again on the shifted planning horizon (Étienne Cuisinier et al., 2022). Figure 2 illustrates the process of the rolling horizon algorithm. Before optimizing, three parameters of the horizon are selected. The schedule horizon (SH) is the planning time horizon of the main problem. The prediction horizon (PH) is the time horizon of considered prediction information taken into account by SAEVs when making a decision. The control horizon (CH) determines how far is the adopted optimized decisions to control the SAEVs into the future. The yellow area in Figure 2 denotes the end states of control, which, after optimization, are passed into the green area, being the initial states in the next optimization. By recording all states of control, we can get the results of the main problem.

Specifically, we apply the method to our model, and the calculation steps are as shown in Figure 3. After the horizons parameters are selected along with the initial state variables and all the parameters in Table 2, the coupled system states within the SH are calculated. Using the rolling horizon algorithm, the problem is decomposed into a number of subproblems, which are solved sequentially. The values of SH and CH determine the number of iterations. At each iteration, we pass the end state within the control range of the previous one into the initial state (line 3 in pseudocode) or input the initial state (line 5). Afterward, the subproblem is computed (line 7), and the system state variables within the control range are recorded (line 8). Figure 3 shows how the state passes between two iterations or subproblems. For example, in the first iteration, we set the initial charging level of vehicle k to 0.2, $q^k_{t_1} = 0.2$, and obtain the change of energy level in the next T_{ph} steps by calculating the first subproblem. The energy level at the T_{Ch} step is passed to the next iteration as the initial energy level, $q^k_{t_2=0} = q^k_{t_1=T_{ch}}$, and the states of the system before T_{ch} are saved as the results of the main problem from $t = 0$ to $t = T_{ch} - 1$, $Q^k_{t=0\to T_{ch}-1} = q^k_{t_1=0\to T_{ch}-1}$. The same is

done for the subsequent iterations.

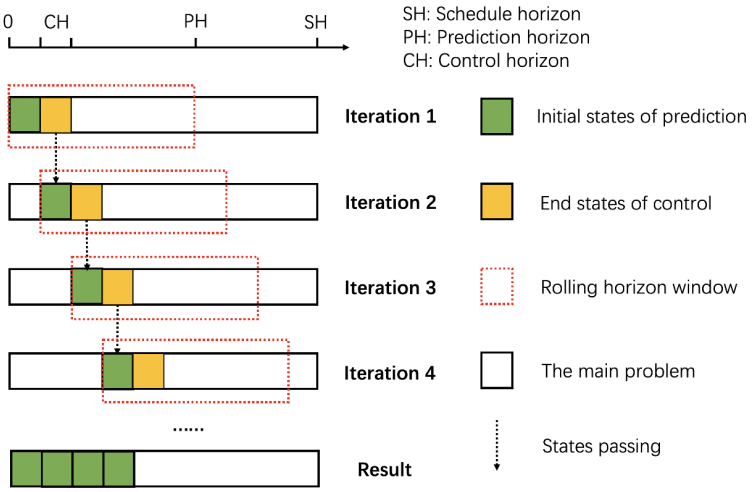

Figure 2: Rolling horizon algorithm

In contrast to the model predictive control algorithm in Zhang et al. (2016), the method here is not only used for the behavioral control of SAEVs but also conveys the state of the grid system. Relying on a rolling horizon algorithm can help to divide a large optimization problem into smaller ones (Étienne Cuisinier et al., 2022). However, although the solution obtained in each prediction horizon is optimal for its subproblem, the results probably are suboptimal for the main problem since information outside the PH is not taken into account. Therefore, PH must be carefully chosen. According to Kopanos and Pistikopoulos (2014), the PH value depends on the problem's characteristics. So, we will discuss the choice of PH as well as CH in the next section considering the model and scenario.

5. Case study

In this section, we present a scenario for evaluating the usefulness of our proposed modeling framework for managing the interdependent SAEV mobility service and power grid system. We propose a case study based on the city of Beijing, China. The aim is to build a realistic scenario that assesses the potential of using SAEVs to facilitate the integration of

Algorithm Rolling Horizon Algorithm

Input: The schedule horizon T_{sh}, the prediction horizon T_{ph}, the control horizon T_{ch}, the initial system state, and the relevant parameters in Table 2.

Output: the System states at each time step within the schedule horizon.

1: **for** $m = 1 \rightarrow \lceil T_{sh}/T_{ch} \rceil^*$ **do**

2: **if** $m \neq 1$ **then**

3: Pass the states. The initial state in the m^{th} iteration is equal to the state at time ${t_{m-1}}^* = T_{ch}$ in the previous iteration.

$$\boldsymbol{\gamma}_{{t_m=0}^*} = \boldsymbol{\gamma}_{t_{m-1}=T_{ch}}$$

4: **else**

5: Input the initial state.

$$\boldsymbol{\gamma}_{t_1=0} = const$$

6: **end if**

7: Solve the subproblem of the coupled model

$$\min_{\substack{i,j \in N \\ t_m=0 \rightarrow T_{ph} \\ k \in V}} \rho_d \sum_{t_m,i,j} d_{i,j,t_m} + \varphi_\omega \sum_{i,j,k,t_m} \tau_{i,j} \omega^k_{i,j,t_m} + \varphi_{sg} \sum_{i,t_m} \mid sg_{i,t_m} \mid$$

$$S.t \qquad Eq.\ (2) \rightarrow (26)$$

8: Save the results from $t_m = 0$ to $t_m = T_{ch} - 1$ as the results of the main problem from $t = (m-1) \times T_{ch}$ to $t = m \times T_{ch}$.

$$\boldsymbol{\Gamma}_{{t=(m-1)\times T_{ch} \rightarrow m \times T_{ch}-1}^*} = \boldsymbol{\gamma}_{t_m=0 \rightarrow T_{ch}-1}$$

9: **end for**

10: **return** The results of the main problem, $\boldsymbol{\Gamma}_t$.

$*$: The symbol denotes round up.

$*$: t_m is the time in the m^{th} subproblem, ranging from 0 to T_{ph}. t is the time in the main problem, ranging from 0 to T_{SH}.

$*$: $\boldsymbol{\gamma}_{t_m}$ is the state vector in the m^{th} subproblem, containing all the state variables in the subproblem.

$$\boldsymbol{\gamma}_{t_m} = [d_{i,j,t_m}\ u^k_{i,t_m}\ ch^k_{i,t_m}\ dc^k_{i,t_m}\ wa^k_{i,t_m}\ p^k_{t_m}\ q^k_{t_m}\ f_{i,j,t_m}\ cd_{i,t_m}\ g_{i,t_m}\ \theta_{i,t_m}\ sg_{i,t_m}]^T$$

$*$: $\boldsymbol{\Gamma}_t$ is the state vector in the main problem, containing all the state variables in the main problem.

$$\boldsymbol{\Gamma}_t = [D_{i,j,t}\ U^k_{i,t}\ CH^k_{i,t}\ DC^k_{i,t}\ WA^k_{i,t}\ P^k_t\ Q^k_t\ F_{i,j,t}\ CD_{i,t}\ G_{i,t}\ \Theta_{i,t}\ SG_{i,t}]^T$$

Figure 3: Rolling horizon algorithm pseudocode

renewable energies into the power grid.

We selected the central region of Beijing as the study area: the Hai Dian, Shi Jing Shan, Feng Tai, Xi Cheng, Dong Cheng, and Chao Yang districts. The centroids of each district are considered to be the origin/destination of the trips in the SAEV system, and the Euclidean distance between them is assumed to be the average distance between two districts so that a simplified 6-node traffic map is generated, as shown in Figure 4. The graph's colors indicate the travel demand between node pairs daily. The travel demand patterns are calculated using the real Taxi GPS dataset from the Python package TransBigData (Yu and Yuan, 2022). More details are available in Appendix A, along with the selection of vehicle parameters.

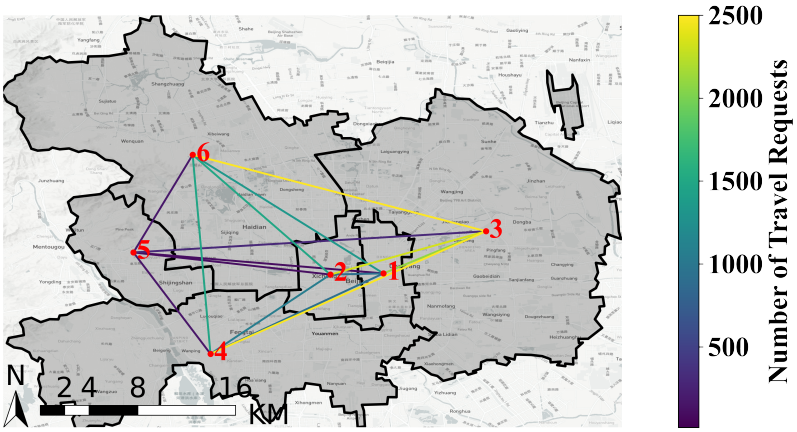

Figure 4: Simplified traffic node map with OD-pairs aggregation

Based on the grid structure of Beijing at the distribution level and some reasonable assumptions, we synthesized a simplified grid as shown in Figure 5. The red nodes in the figure are the centroids of the districts, which means we ignore the power transmission within the regions and simplify the distribution of power stations. The connecting lines represent the sum of power transmission lines between regions, where the main line type is 220 Kv. In Appendix B, we detail the synthesis process and the selection of the grid system parameters. Further, we present the renewable energy capacity factor calculation based on climate data in Appendix C. Multiplying the capacity factor by the installed capacity of the renewable energy source gives the predicted electricity production values, which provides a calculation

scenario for the potential analysis of SAEV to help the grid integration of renewable energy resources.

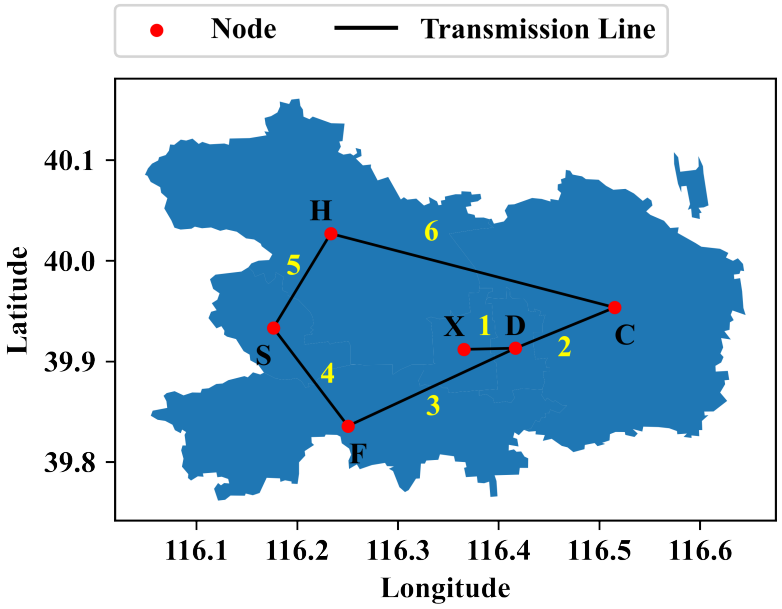

Figure 5: The synthetic power grid in Beijing

When using the rolling horizon algorithm, the original problem is decomposed into a number of subproblems. The choice of PH and CH plays an important role in the performance of our algorithm. We choose PH = 4 and CH = 1, according to the process described in Appendix D.

6. Results and discussion

In this section, we use the rolling horizon algorithm to compute the results based on the case study as described before. We further discuss and analyze the results. All computational experiments are performed on a MacBook running macOS Monterey 12.4, using the Apple M1 chip, 8 GB of RAM, and Gurobi 9.5.1 is used as MIP solver.

6.1. Objective function weight and penalties

Before the calculation, we also need to set the weight and penalties of the objective function. In Zhang et al. (2016), the objective function weight is set to 1 by default, and the penalty weight of vehicle rebalancing is set to a small value. In our model, we set the weight of the objective term of SAEV based on the Beijing Taxi service price, as shown in Table 3. The rebalancing cost of SAEV is set to 1 Yuan/Km, which is a reasonable value based on the service price. Thus, the objective term represents the potential benefit yet to be gained, and the second penalty term represents the economic cost of rebalancing. the SAEV always makes the choice of maximizing the economic benefit. As for the penalty term for interaction with the grid, we set it to a small value of 0.0001 to prioritize the transportation service for SAEVs.

Table 3: Travel price

Distance	≤ 3 Km	3-15 Km	≥ 15 Km
Price	10 yuan	2 yuan/Km	3 yuan/Km

6.2. Model validation

In this part, we calculate a regulation problem described in Zhang et al. (2016). The regulation problem verifies the analytic stability of the model and algorithm, and the proof process is extensively detailed in that paper. We also undertake a charging rate impact experiment, which serves two primary purposes: First, it allows us to explore the influence of the vehicle charging rate on the system's service performance. Second, it serves as a validation test to prove the robustness of our model and algorithm in the presence of external disturbances (travel demands). This part affirms the viability of our model and algorithm for further experiments. It is necessary to state that in the calculation, in order to scale the SAEV system to the grid system, we use a factor of 100, i.e., the behavior of one vehicle in our model represents the behavior of 100 SAEVs in reality. Thus, in this paper, one electric vehicle (representing 100 vehicles with 100 kWh battery capacity) may lead to a 10 MWh charging demand for the grid. This is reasonable statistically, considering the geographic

scale and temporal resolution we set. In the subsequent discussion, we only present the vehicle number that has been multiplied by the scaling factor for the sake of description consistency. The parameter settings for the calculations are summarized in Table 4.

Table 4: Parameters settings in the model validation

Experiment	Model validation	Impact of charging rate
Time Resolution (min)	30	30
Initial Energy	0.2	0.2
Vehicle Number	1800	1200
Charging Rate	0.06	0.06/0.12/0.25/0.4
Discharging Rate	-	0.25
Consumption Rate	0.3	0.3
Battery Capacity	100	100
Travel Demand	7500 initial passengers	Dynamic pattern in Appendix A
RES Penetration	-	-
Power Grid Configuration	-	Scenario in Appendix B

In the regulation problem calculation, the time resolution is set to 30 minutes, with charging and consumption power at 12 kW and 6 kW, respectively. The initial energy storage of the SAEV is established at 20 kWh, with a battery capacity of 100 kWh, resulting in an initial energy level of 0.2. According to the definition, the charging rate can be expressed by Eq.(47).

$$ChargingRate = \frac{ChargingPower \times TimeResolution}{BatteryCapacity} \tag{47}$$

Therefore, the charging rate is 0.06. It's the same for consumption rate, which is 0.03. Each node starts with a distribution of 300 SAEVs and 7500 passengers waiting to be picked up and dropped off at the other 5 nodes. New travel demand is not considered here. The results are shown in Figure 6. The decrease in travel demand over time demonstrates the analytic stability of the SAEV model and algorithm. The fastest decrease happens at node 2 and the slowest at node 6, which demonstrates the geographical features in our Beijing case. Node 2 denotes the center region, Xicheng district, which is close to other nodes, and node 6 denotes the peripheral one, Hai Dian district, which is rather far from others. Figure 6b shows the evolution of the state of charge of the SAEV system, in which the charge of SAEVs changes periodically, causing periodic pauses in the decrease of demands. The consistency between the calculation results and input data, as well as the relationships among variables,

further confirm the correctness of the model.

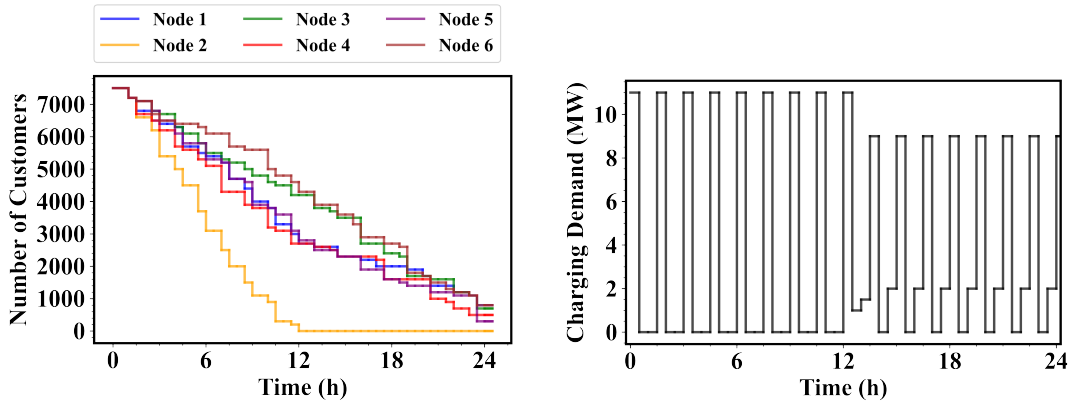

(a) Number of waiting customers at each station

(b) State of charge of vehicles

Figure 6: Results of the regulation problem

We also explored the impact of charging rate on the transport service of the SAEV system, which, according to the literature, varies with regards to the chargers used. In this test, the average waiting time (AWT) was defined as a measure of the transport performance of the SAEVs and is represented by Eq.(48). $\sum_{i,j,t} d_{i,j,t}$ denotes the sum of the waiting passengers recorded every 30 minutes until time t, multiplied by 30 minutes, which further denotes the total length of time passengers have been waiting. This is then divided by the total number of travel demands to obtain the average waiting time for a passenger.

$$AWT = 30min \times \frac{\sum_{i,j,k} d_{i,j,k}}{\sum_{i,j,k} c_{i,j,k}} \tag{48}$$

We calculated the charging power at 12 Kw, 24 Kw, 50 Kw, and 80 Kw, which corresponds to charging rates of 0.06, 0.12, 0.25, and 0.4, respectively as per Eq.(47). Each node is assigned 200 SAEVs for this test with an initial charging rate of 0.2. To ensure a robust analysis, we utilized a random selection process to generate 10 distinct travel demand patterns for 1200 Taxis. For each charging rate scenario, we input these travel demand characteristics and conducted 10 separate calculations. The calculation results are shown in the box plot in Figure 7. The length of the box indicates the range of the 10 calculation results, and the orange line segment in the middle represents the median value of the calculation

results.

It can be seen that the result of AWT of 0 exists for all four charging rates we set, which indicates that the SAEV system can perfectly solve the travel demand characteristics faced at this point. However, when the charging rate is set to 0.06, the median AWT equals 40.5 min, and the highest value exceeds 250 min, which suggests that the SAEV system performs poorly in most cases when the charging rate is 0.06. When the charging rate is doubled to 0.12, the median AWT value drops to 10.9 min, which is 73% less than before, and the maximum value decreases to about 100 min. This indicates that the increase in charging rate enhances the quality of service of the SAEV system. We further increase the rate to 0.25 and 0.4, and although the maximum value of AWT still decreases significantly, the median AWT gradually stabilizes at around 10 minutes. This is because for the case of low travel demand, the charging rate of 0.12 is already able to satisfy the charging demand of the SAEV system, and the waiting time is mainly caused by the incongruity between travel demand characteristics and vehicle distribution and thus is no longer affected by the charging rate. These findings are consistent with those in the literature (Zhang et al., 2016; Chen et al., 2016; Vosooghi et al., 2020; Bauer et al., 2018)

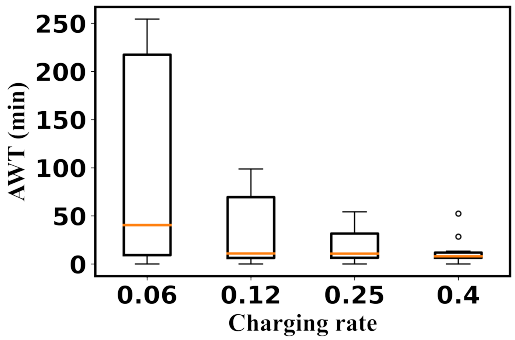

Figure 7: Average Waiting Time (AWT) with different charging rates

6.3. Integration of renewable energy sources (RES) in the power grid

This section explores the potential of SAEVs to help grid integration of renewable energy sources. The coupled system is simulated under different scenarios, including different re-

newable energy penetration rates and SAEV fleet sizes. The renewable energy penetration rate is calculated by the installed capacity of renewable energy resources divided by the overall generation capacity of the power system. It should be noted that the renewable energy sources we consider include both wind and solar-PV energy, and their installed capacity ratio is assumed to be 1 to 1. This ratio affects the power production characteristics of the grid system as does the installed capacity, since the capacity factors for wind and solar vary considerably. However, the effect of this factor is not considered in this paper because it is not relevant to the subject of this paper, and therefore, the ratio is always kept as 1 to 1. Additionally, the fleet size of SAEV depends on the number of vehicles, as we assume that the SAEV system will face a dynamic travel demand, calculated from the Taxi GPS dataset, as done in section 6.2. To ensure a robust analysis, we generated 10 distinct travel demand patterns and conducted 10 separate calculations for each scenario. The resulting average value forms the basis for all subsequent discussions. The parameter settings for the calculations are summarized in Table 5.

Table 5: Parameters settings in the integration of RES in the power grid

Experiment	Performance in different fleet sizes	Performance in different RES penetration
Time Resolution (min)	30	30
Initial Energy	0.2	0.2
Vehicle Number	0/4200/4800/5400	0/4800/5400/7200
Charging Rate	0.25	0.25
Discharging Rate	0.25	0.25
Consumption Rate	0.3	0.3
Battery Capacity	100	100
Travel Demand	Dynamic pattern in Appendix A	Dynamic pattern in Appendix A
RES Penetration	4.1%	Increasing from 3.9%
Power Grid Configuration	Scenario in Appendix B	Scenario in Appendix B

In the test, we fixed the penetration of renewable energy in the grid at 4.1% and calculated the performance of the coupled system in terms of traffic service and power balance for different fleet sizes, 4200, 4800, and 5400 SAEVs. More specifically, 140 MW of installed conventional generation capacity is replaced by renewable energy sources, including 70 MW of solar PV and 70 MW of wind power. Based on the assumption of distributed installations, they are distributed in different areas according to the area ratio. The hourly generation of renewable energy sources is shown in Figure 8a (green line), where the generation pattern is

similar to the hourly capacity factor of solar-PV since wind energy is very low in our case. To overcome the intermittency of renewable energy sources, the grid constantly adjusts the generation of conventional energy sources, reducing them when there is more renewable energy production and increasing them when the opposite is true. In this way, the grid balances production and consumption, effectively using conventional plants as a backup for renewable energy generation. Without the involvement of SAEV, the grid can be balanced for most of the day when the renewable energy penetration is 4.1%, but as shown in 8b, an energy shortage occurs between 19:00 and 21:00. From the comparison of generation and consumption in Figure 8a, the reason is that the low production of renewable energy does not match the high consumption during this time, and the conventional power plants cannot do much even if they maintain their maximum output. The largest power shortage is 11.87 MW.

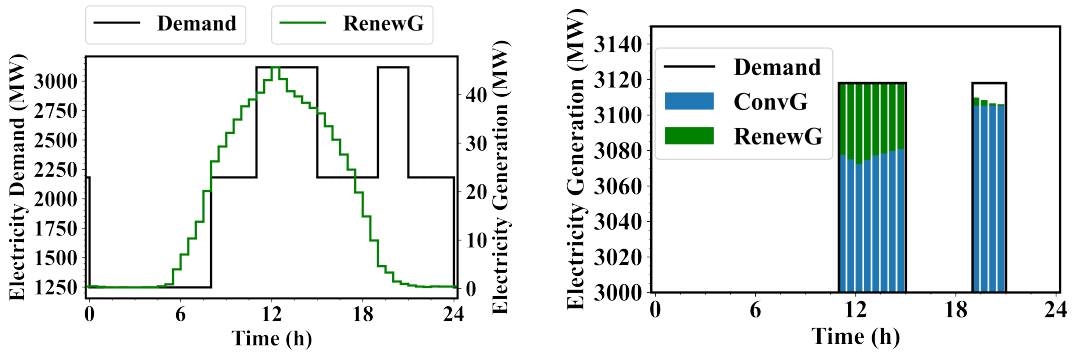

(a) Hourly generation

(b) Hourly load

Figure 8: Hourly generation and load without SAEVs

First, a fleet of 4200 SAEVs is considered. According to the vehicle parameters, the charging and discharging rates are set to 0.25, which means that the SAEVs use fast charging technology. The consumption rate was set to 0.03. The system started operation at 00:00 when the initial energy levels of the SAEVs were all set to 0.2. This is a reasonable estimate since the energy levels of the vehicles are usually low after a day of work.

The obtained results reveal key insights into SAEVs' behavior when interacting with the grid. Figure 9a shows the variation in average travel demand and waiting customers

throughout the day. Notably, there is a distinct cutoff in travel demand at 10:00, with low demand before and high demand after. With a renewable energy penetration of 4.1%, 4200 SAEVs efficiently meet most of the demand. However, from 18:00 to 22:00, the number of waiting customers increased significantly, peaking at 1100, due to power shortages in the grid system.

Figure 9b depicts the SAEV charging process, revealing that before the power shortage, the system peaks at 32 MW to prepare for the crisis. Despite the energy shortage, most SAEVs prioritize passenger transportation over grid energy supply during crisis hours. As a result, only 2.5 MW is discharged between 19:00 and 19:30, leaving a significant 11.87 MW power shortage. As the grid system lacks the capacity to recharge SAEVs during this period, some vehicles are unable to replenish energy after transporting passengers, causing an increase in waiting passengers. After the crisis, the SAEV system requires time to recharge, leading to additional waiting periods. In summary, with a fleet size of 4200, the SAEV system fails to support grid integration of 4.1% renewable energy and degrades its own transportation service levels.

Next, we increased the fleet size to 4800 and 5400 by adding 100 and 200 SAEVs at each node, respectively, and calculated the operation results. Figure 10 compares the scenarios for three different fleet sizes and when no SAEVs are involved. To focus on the period around the power shortage, we present only the calculated results from 18:00 to 23:00. The graph on the right records the value of the power shortage in the grid system, where zero indicates a balanced supply and demand, and -8 indicates an 8 MW power demand exceeding the actual supply. Observing the graph, we find that the travel demand can be met with a fleet size of 4800, and the maximum shortage is reduced to 9.5 MW, although the problem is not fully resolved. However, with a fleet size of 5400 vehicles, the SAEV system exhibits excellent performance in both traffic and grid aspects. Not only is the travel demand satisfied, but the power system also experiences no shortages. Consequently, the SAEV system with a fleet size of 5400 SAEVs can safely support the integration of 4.1% of renewable energy sources into the grid.

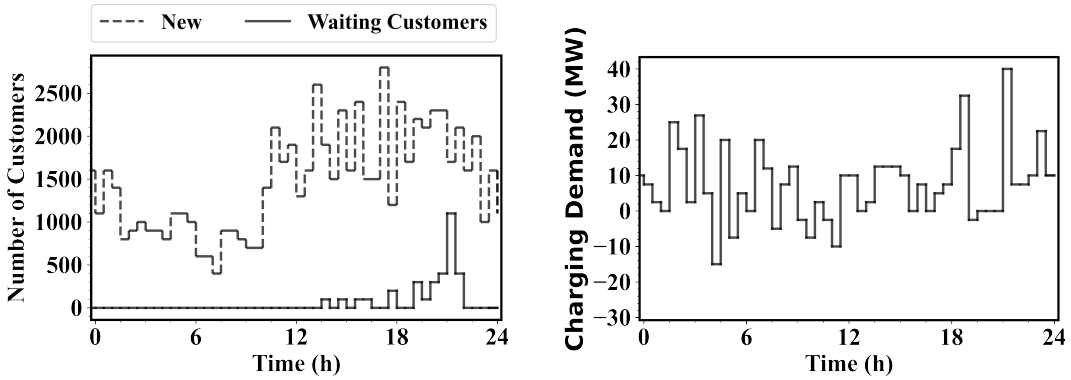

(a) Hourly number of waiting customers

(b) Hourly charging demand of vehicles

Figure 9: Performance of SAEV system with 4200 SAEVs

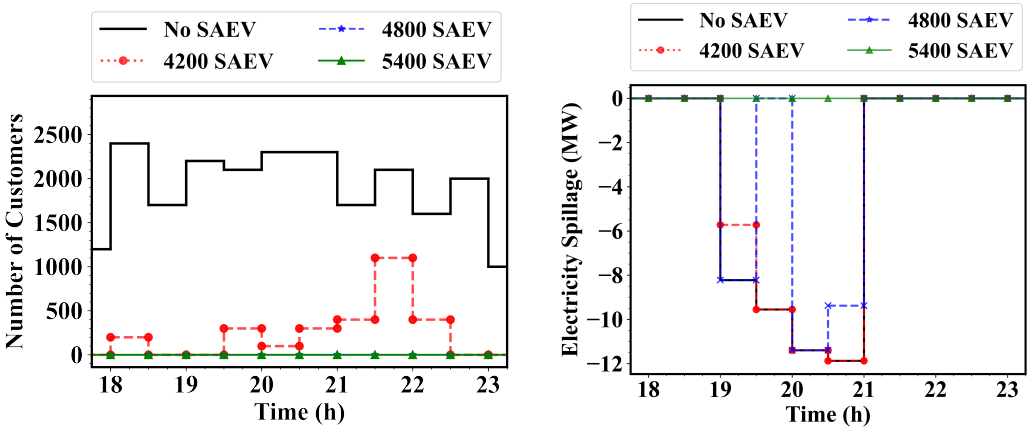

(a) Hourly number of waiting customers

(b) Hourly energy shortage of power grid

Figure 10: Performance of SAEV system with different SAEV fleet size

In the next test, we fix the fleet size and adjust the renewable energy resources penetration rate until the grid system does not experience power shortages. Table 6 gives the acceptable renewable energy sources penetration rates for the grid system with the help of SAEV fleets of different sizes. In our case, the grid utilizes conventional energy as a backup source and can safely integrate 3.9% of renewable energy itself. Even with the help of 4800 SAEVs, the penetration rate cannot be further increased. As mentioned before, when the fleet size is 4200 and 4800, SAEVs are busy transporting customers and do not have much excess energy to feed the grid. In addition, when the fleet size increases to 5400, the accept-

able penetration rate is 4.1%, which increases to 4.4% when there are 7200 SAEVs. The above shows that SAEV systems have great potential to help integrate renewable energy into the grid, and the larger the fleet size, the more renewable energy can be connected to the grid. However, an increase in fleet size results in higher investment costs, and scaling up without substantial benefits to the grid system would be impractical. Setting the fleet size to exactly match the travel demand (4800 SAEVs) would lower investment costs; however, failing to assist the grid effectively could lead to additional expenses. Hence, it would be interesting to value vehicles and the grid in financial terms to evaluate the economic viability. This will be subject to investigation in future work.

Table 6: Acceptable penetration rate of RES in different SAEV fleet sizes

No SAEV	4800 SAEVs	5400 SAEVs	7200 SAEVs
3.9%	3.9%	4.1%	4.4%

6.4. Model comparison and sensitivity analysis

In this part, we conducted a comparison between the isolated SAEV transportation model and the coupled model incorporating the power grid, focusing on the scenario described in the preceding subsection, which involves 4200 vehicles and a 4.1% penetration of renewable energy, and also a sensitivity analysis to the discharging rate, consumption rate and battery capacity of SAEVs. The parameter settings for the calculations are summarized in Table 7.

Figures 11 illustrate the comparison of the number of waiting customers and the evolution of vehicle charging demand during key time intervals. From the Figure 11a, it is evident that SAEVs consistently meet all travel demands, resulting in zero waiting customers at all times. This outcome is rational, as SAEVs maintain a steady charging profile unaffected by constraints from the power grid, as depicted in the Figure 11b. Even during periods of electricity shortage, from 19:00 to 21:00, SAEVs continue charging, ensuring they always possess ample energy reserves to meet incoming travel demands. In contrast, the charging pattern of SAEVs in the coupled model displays notable fluctuations. This difference highlights the importance of considering the coupled model. Neglecting the constraints of the

Table 7: Parameters settings in the model comparison and sensitivity analysis

Experiment	Isolated model vs coupled model	Discharging rate	Consumption rate	Battery capacity
Time Resolution (min)	30	30	30	30
Initial Energy	0.2	0.2	0.2	0.2
Vehicle Number	4200	4200	4200	4200
Charging Rate	0.25	0.25	0.25	0.25
Discharging Rate	0.25	0.06/0.12/0.25/0.4	0.25	0.25
Consumption Rate	0.3	0.3	0.01/0.03/0.06/0.09	0.03
Battery Capacity	100	100	100	60/80/100/120
Travel Demand	Dynamic pattern in Appendix A	Dynamic pattern in Appendix A	Dynamic pattern in Appendix A	Dynamic pattern in Appendix A
RES Penetration	4.1%	4.1%	4.1%	4.1%
Power Grid Configuration	Scenario in Appendix B	Scenario in Appendix B	Scenario in Appendix B	Scenario in Appendix B

power grid poses a risk of overestimating the service performance of SAEVs. Furthermore, the charging patterns of SAEVs may not synchronize with the operational dynamics of the power grid, potentially imposing additional strain on the power system.

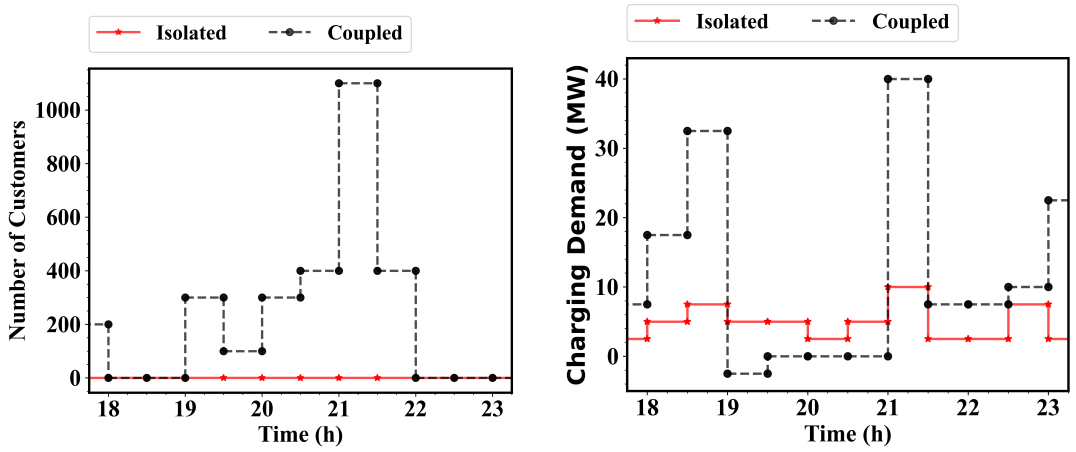

(a) Hourly number of waiting customers

(b) Hourly charging demand of vehicles

Figure 11: Performance of SAEV system calculated by different model

A sensitivity analysis was also performed on the coupled model to examine the impact of key parameters on SAEV service efficiency, specifically focusing on average waiting time (AWT) for customers and the discharging capacity of vehicles to the power grid. Each parameter was tested across four different vehicle numbers (4200, 4800, 5400, and 7200).

The analysis of charging rate was previously performed in the model validation section. The effects of varying vehicle discharging rates are depicted in Figure 12a. It's observed that a higher discharging rate leads to increased discharging electricity from SAEVs as expected, but it also raises the AWT due to reduced available energy caused by the higher discharging energy. Figure 12b illustrates the influence of different consumption rates, which exhibit a strong correlation with AWT and a negative correlation with discharging capacity. Unlike consumption rate, battery capacity appears to primarily affect discharging capacity with minimal impact on AWT, as shown in Figure 12c. The results of the sensitivity analysis further underscore the importance of integrating considerations from both the transportation and power systems. For instance, when selecting the discharging rate for SAEVs, it's crucial to strike a balance between both aspects. Battery capacity should be increased in accordance with its relation to discharging capacity, even though it has little effect on travel service efficiency. Moreover, from the result of consumption rate, it is evident that when designing SAEVs, striving for lower energy consumption is always an excellent choice.

7. Conclusion

The existing body of research on the combined management of Shared Autonomous Electric Vehicles (SAEVs) considering electric power systems constraints presents a significant gap with regard to providing comprehensive modeling, optimization, and assessment approaches that consider both transportation and electric power systems. This deficiency has led to an oversimplification of grid-related aspects, often focusing on problems related to planning charging infrastructure. Consequently, the broader scope of SAEV contributions to grid integration, particularly in facilitating the incorporation of renewable energy sources, has been largely overlooked.

The present study presents a structured modeling and optimization framework that considers both transportation and grid systems and explores the potential of SAEVs to enhance the integration of renewable energy sources into the grid. To achieve this, the study extends the existing SAEV Mobility-on-demand mode in Zhang et al. (2016) by coupling it with a DC-Optimal Power Flow power system model.

Some specific operation scenarios are designed based on the collected data on traffic, power grid, and climate in Beijing. Using the parameters in the scenarios as inputs to the model, we calculate the operation results of the coupled system under these scenarios. The validity of the model is illustrated by the calculation of the regulation problems and charging rate impact experiments. By examining the relationship between the penetration rate of renewable energy sources to the grid system and the size of the SAEV fleet, we illustrate that SAEVs have the potential to help connect renewable energy sources to the grid. Additionally, we compare the performance of the isolated SAEV transportation model with the SAEV-PS coupled model to underscore the necessity of considering the latter. Furthermore, a sensitivity analysis is performed on the coupled model to assess the impact of key parameters on SAEV service efficiency. It should be emphasized that the modeling and optimization framework presented in this paper can be easily generalized to case studies other than the one chosen in our paper, making it adaptable to a diverse set of scenarios.

However, for some expansive scenarios, the current approach in this paper may encounter computational barriers. To address this, we plan to employ approximate dynamic programming to reformulate the framework for scalability. Future endeavors will extend beyond, incorporating the impact of climate change and extreme weather in the model. This extension aims to cultivate a more resilient management strategy for the SAEV-grid coupled system, providing indispensable policy insights over an extended timeframe.

References

Abdin, A.F., Caunhye, A., Zio, E., Cardin, M.A., 2022. Optimizing generation expansion planning with operational uncertainty: A multistage adaptive robust approach. Applied Energy 306, 118032.

Abdin, A.F., Zio, E., 2018. An integrated framework for operational flexibility assessment in multi-period power system planning with renewable energy production. Applied Energy 222, 898–914.

Abdin, A.F., Zio, E., 2019. Optimal Planning of Electric Power Systems. Springer International Publishing, Cham. pp. 53–65.

Aigner, K.M., Schaumann, P., von Loeper, F., Martin, A., Schmidt, V., Liers, F., 2022. Robust dc optimal power flow with modeling of solar power supply uncertainty via r-vine copulas. Optimization and Engineering 24, 1951–1982.

Anees, A.S., 2012. Grid integration of renewable energy sources: Challenges, issues and possible solutions, in: 2012 IEEE 5th India International Conference on Power Electronics (IICPE), IEEE, Delhi, India. pp. 1–6.

Azzopardi, B., 2014. Green energy and technology: Choosing among alternatives, in: Hossain, J., Mahmud, A. (Eds.), Renewable Energy Integration: Challenges and Solutions. Springer, Singapore, pp. 1–16.

Bauer, G.S., Greenblatt, J.B., Gerke, B.F., 2018. Cost, energy, and environmental impact of automated electric taxi fleets in manhattan. Environmental Science and Technology 52, 4920–4928.

Bischoff, J., Maciejewski, M., 2016. Simulation of city-wide replacement of private cars with autonomous taxis in berlin. Procedia Computer Science 83, 237–244.

Bélanger, V., Ruiz, A., Soriano, P., 2019. Recent optimization models and trends in location, relocation, and dispatching of emergency medical vehicles. European Journal of Operational Research 272, 1–23.

Carpentier, J., 1979. Optimal power flows. International Journal of Electrical Power & Energy Systems 1, 3–15.

Chen, T.D., Kockelman, K.M., Hanna, J.P., 2016. Operations of a shared, autonomous, electric vehicle fleet: Implications of vehicle & charging infrastructure decisions. Transportation Research Part A: Policy and Practice 94, 243–254.

Étienne Cuisinier, Lemaire, P., Penz, B., Ruby, A., Bourasseau, C., 2022. New rolling horizon optimization approaches to balance short-term and long-term decisions: An application to energy planning. Energy 245, 122773.

Ding, Y., Li, X., Jian, S., 2022. Modeling the impact of vehicle-to-grid discharge technology on transport and power systems. Transportation Research Part D: Transport and Environment 105, 103220.

Fagnant, D.J., Kockelman, K.M., 2014. The travel and environmental implications of shared autonomous vehicles, using agent-based model scenarios. Transportation Research Part C: Emerging Technologies 40, 1–13.

Fernandes, C., Frías, P., Latorre, J.M., 2012. Impact of vehicle-to-grid on power system operation costs: The spanish case study. Applied Energy 96, 194–202. Smart Grids.

Fulton, L.M., 2018. Three revolutions in urban passenger travel. Joule 2, 575–578.

Grazia Speranza, M., 2018. Trends in transportation and logistics. European Journal of Operational Research 264, 830–836.

Han, S., Han, S., Sezaki, K., 2010. Development of an optimal vehicle-to-grid aggregator for frequency regulation. IEEE Transactions on Smart Grid 1, 65–72.

Heide, D., von Bremen, L., Greiner, M., Hoffmann, C., Speckmann, M., Bofinger, S., 2010. Seasonal optimal mix of wind and solar power in a future, highly renewable europe. Renewable Energy 35, 2483–2489.

Huang, Y., Liu, J., Shen, X., Dai, T., 2013. The interaction between the large-scale evs and the power grid. Smart Grid and Renewable Energy 4, 137–143.

Iacobucci, R., McLellan, B., Tezuka, T., 2018a. Modeling shared autonomous electric vehicles: Potential for transport and power grid integration. Energy 158, 148–163.

Iacobucci, R., McLellan, B., Tezuka, T., 2018b. The synergies of shared autonomous electric vehicles with renewable energy in a virtual power plant and microgrid. Energies 11.

Iacobucci, R., McLellan, B., Tezuka, T., 2019. Optimization of shared autonomous electric vehicles operations with charge scheduling and vehicle-to-grid. Transportation Research Part C: Emerging Technologies 100, 34–52.

IEA, 2022. World Energy Outlook 2022. Technical Report License: CC BY 4.0. International Energy Agency. Paris, France.

Ikezoe, K., Kiriyama, E., Fujimura, S., 2020. Car-sharing intention analysis in japan by comparing the utility of car ownership for car-owners and non-car owners. Transport Policy 96, 1–14.

Kang, D., Levin, M.W., 2021. Maximum-stability dispatch policy for shared autonomous vehicles. Transportation Research Part B: Methodological 148, 132–151.

Khodayar, M.E., Wu, L., Li, Z., 2013. Electric vehicle mobility in transmission-constrained hourly power generation scheduling. IEEE Transactions on Smart Grid 4, 779–788.

Kopanos, G.M., Pistikopoulos, E.N., 2014. Reactive Scheduling by a Multiparametric Programming Rolling Horizon Framework: A Case of a Network of Combined Heat and Power Units. Industrial & Engineering Chemistry Research 53, 4366–4386.

Li, X., Ma, J., Cui, J., Ghiasi, A., Zhou, F., 2016. Design framework of large-scale one-way electric vehicle sharing systems: A continuum approximation model. Transportation Research Part B: Methodological 88, 21–45.

Liu, Z., Miwa, T., Zeng, W., Bell, M.G., Morikawa, T., 2018. Shared Autonomous Taxi System and Utilization of Collected Travel-Time Information. Journal of Advanced Transportation 2018, 8919721.

Loeb, B., Kockelman, K.M., Liu, J., 2018. Shared autonomous electric vehicle (saev) operations across the austin, texas network with charging infrastructure decisions. Transportation Research Part C: Emerging Technologies 89, 222–233.

Ma, J., Li, X., Zhou, F., Hao, W., 2017. Designing optimal autonomous vehicle sharing and reservation systems: A linear programming approach. Transportation Research Part C: Emerging Technologies 84, 124–141.

Motta, V.N., Anjos, M.F., Gendreau, M., 2023. Survey of optimization models for power system operation and expansion planning with demand response. European Journal of Operational Research .

Mwasilu, F., Justo, J.J., Kim, E.K., Do, T.D., Jung, J.W., 2014. Electric vehicles and smart grid interaction: A review on vehicle to grid and renewable energy sources integration. Renewable and Sustainable Energy Reviews 34, 501–516.

Noel, L., de Rubens, G., Kester, J., Sovacool, B., 2017. The Status and Challenges of Electric Vehicles in Norway–2017. Technical Report. Aarhus University School of Business and Social Sciences Department of business development and technology. Aarhus, Denmark.

Richardson, D.B., 2013. Electric vehicles and the electric grid: A review of modeling approaches, impacts, and renewable energy integration. Renewable and Sustainable Energy Reviews 19, 247–254.

Sun, B., Sun, X., Tsang, D.H., Whitt, W., 2019. Optimal battery purchasing and charging strategy at electric vehicle battery swap stations. European Journal of Operational Research 279, 524–539.

Vosooghi, R., Puchinger, J., Bischoff, J., Jankovic, M., Vouillon, A., 2020. Shared autonomous electric vehicle service performance: Assessing the impact of charging infrastructure. Transportation Research Part D: Transport and Environment 81, 102283.

Vosooghi, R., Puchinger, J., Jankovic, M., Vouillon, A., 2019. Shared autonomous vehicle simulation and service design. Transportation Research Part C: Emerging Technologies 107, 15–33.

W Axhausen, K., Horni, A., Nagel, K., 2016. The multi-agent transport simulation MATSim. Ubiquity Press, London, UK.

Wang, D., Liao, F., 2021. Analysis of first-come-first-served mechanisms in one-way car-sharing services. Transportation Research Part B: Methodological 147, 22–41.

Wolinetz, M., Axsen, J., Peters, J., Crawford, C., 2018. Simulating the value of electric-vehicle-grid integration using a behaviourally realistic model. Nature Energy 3, 132–139.

Xu, Y., Pan, F., 2012. Scheduling for charging plug-in hybrid electric vehicles, in: 2012 IEEE 51st IEEE Conference on Decision and Control (CDC), IEEE, Maui, HI, USA. pp. 2495–2501.

Yao, X., Fan, Y., Zhao, F., Ma, S.C., 2022. Economic and climate benefits of vehicle-to-grid for low-carbon transitions of power systems: A case study of china's 2030 renewable energy target. Journal of Cleaner Production 330, 129833.

Yi, Z., Bauer, P.H., 2016. Spatiotemporal energy demand models for electric vehicles. IEEE Transactions on Vehicular Technology 65, 1030–1042.

Yu, Q., Yuan, J., 2022. Transbigdata: A python package for transportation spatio-temporal big data processing, analysis and visualization. Journal of Open Source Software 7, 4021.

Zhang, R., Rossi, F., Pavone, M., 2016. Model predictive control of autonomous mobility-on-demand systems, in: IEEE International Conference on Robotics and Automation (ICRA), IEEE, Stockholm, Sweden. pp. 1382–1389.

Zhang, T.Z., Chen, T.D., 2020. Smart charging management for shared autonomous electric vehicle fleets: A Puget Sound case study. Transportation Research Part D: Transport and Environment 78, 102184.

Zhang, W., Guhathakurta, S., Fang, J., Zhang, G., 2015. Exploring the impact of shared autonomous vehicles on urban parking demand: An agent-based simulation approach. Sustainable Cities and Society 19, 34–45.

Zhou, F., Zheng, Z., Whitehead, J., Perrons, R.K., Washington, S., Page, L., 2020. Examining the impact of car-sharing on private vehicle ownership. Transportation Research Part A: Policy and Practice 138, 322–341.

Özkan, E., 2020. Joint pricing and matching in ride-sharing systems. European Journal of Operational Research 287, 1149–1160.

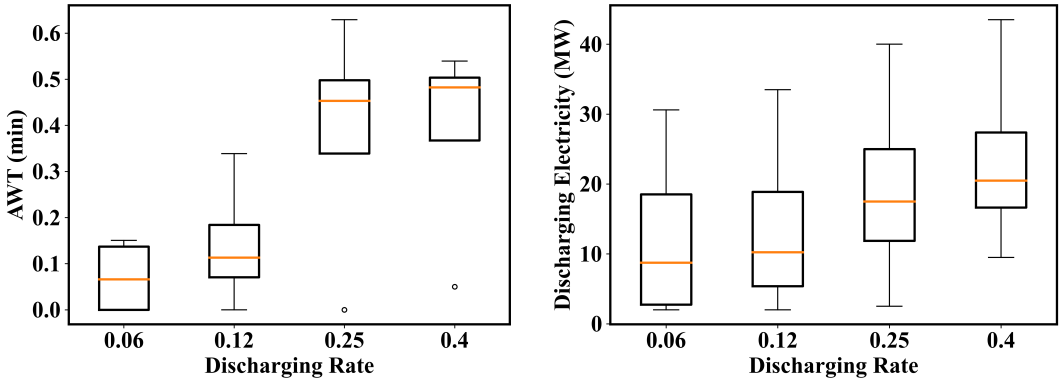

(a)

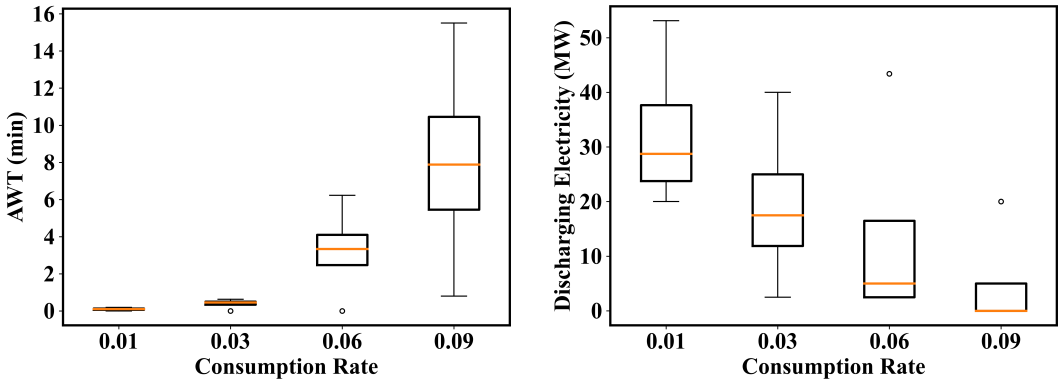

(b)

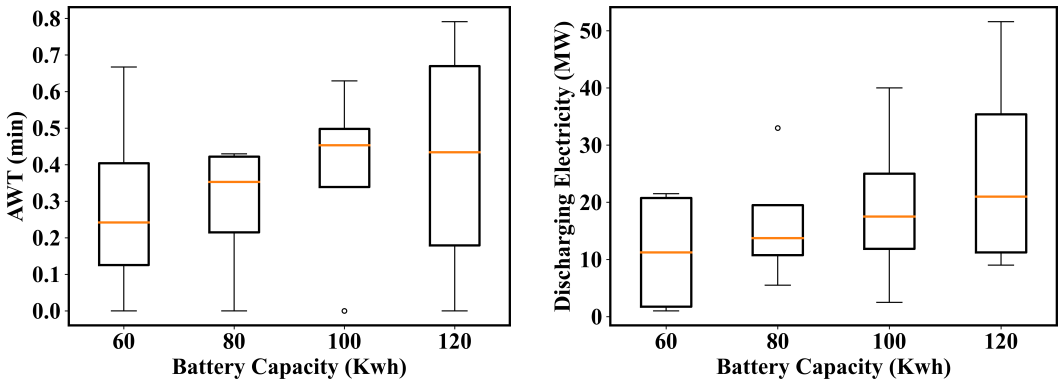

(c)

Figure 12: Sensitivity of Average Waiting Time (AWT) of customers and discharging capacity of vehicles for different parameters: (a) discharging rate; (b) consumption rates; (c) battery capacity.